NASA Technical Paper 1841

Forced and Natural Convection in Laminar-Jet Diffusion Flames

John B. Haggard, Jr.

JUNE 1981

NASA

NASA Technical Paper 1841

Forced and Natural Convection in Laminar-Jet Diffusion Flames

John B. Haggard, Jr.
Lewis Research Center
Cleveland, Ohio

NASA
National Aeronautics
and Space Administration

Scientific and Technical
Information Branch

1981

Summary

An experimental investigation was conducted on methane, laminar-jet, diffusion flames with coaxial, forced air flow to examine the shapes of normal-gravity, zero-gravity, and inverted-gravity flames. Fuel nozzles ranged in size from 0.051 to 0.305-cm inside radius, while the coaxial, convergent air nozzle had a 1.4-cm inside radius at the fuel-exit plane. Fuel flows ranged from 1.55 to 10.3 cm^3/sec, and air flows from 0 to 597 cm^3/sec. A computer program developed under a previous government contract calculated characteristic dimensions of normal- and zero-gravity diffusion flames only. The comparison between the experimental data and the computed axial flame lengths for normal gravity and zero gravity showed good agreement. The inverted-gravity, maximum flame radius was proportional to the nozzle radius and the logarithm of the ratio of nozzle radius to average fuel velocity. Flame extinguishment upon entry into weightlessness was studied, and it was found that relatively low forced air velocities ($\approx$ 10 cm/sec) are sufficient to sustain methane flame combustion in zero gravity. Flame color is also discussed.

Introduction

The NASA Lewis Research Center, as part of its fire research program, has been concerned with burning as it occurs in a weightless environment. Because of the absence of buoyancy in zero gravity, the normal processes of mixing and product cleansing of the flame are altered. These changes may require designers to use different fire-detection and fire-extinguishment hardware and procedures to properly safeguard an orbiting spacecraft. Therefore, an effort is being made to examine the burning of many different types of fuels in several typical spacecraft atmospheres and gravity fields.

The measurement and observation of flame spread rates over surfaces (refs. 1 to 3) have shown that burning in zero gravity is generally slower and less intense than in normal gravity. Studies of gas-jet diffusion flames in an open, quiescent environment (refs. 4 to 10) have shown that such flames burning in air at zero gravity display a wide range of behavior. These types of flames must be considered as a possible fire source within vehicles carrying pressurized fuel gases. Generally, these flames fall into three classes: (1) Steady-state flames that occur on small nozzles and at high fuel flow rates, (2) transient flames which occur on large nozzles and at low fuel flow rates, and (3) self-extinguishing flames which occur on large nozzles and at very low fuel rates. While the first two conditions have been observed with methane, hydrogen, ethylene, and propylene, the third condition has been observed only when methane was the fuel. The transient flames may well be the result of an insufficient maximum operating test time (2.2 sec) and do not necessarily indicate inherrently-unstable-combustion and/or fluid-dynamics problems. For the study of steady-state flames, reference 10 documents correlations between the axial length and the maximum radius of the flames for several hydrocarbon and hydrogen fuels.

References 1 to 10 provide a good basic background for the general study of diffusion flames in zero gravity; yet, an initially quiescent atmosphere may not be a practical test environment. In an orbiting spacecraft, even small, stray, room currents from personnel moving about or the currents from an air-conditioning system could provide enough moving air near a flame to significantly alter its burning characteristics in zero gravity.

A number of researchers have examined the classic Burke-Shulman, gas-jet, diffusion-flame problem. For example, Kimura and Ukawa (ref. 11) have found that normal-gravity, city-gas flames in quiescent environment were 1.5 times longer than flames in confined, coaxial air stream with the same average velocity as the fuel.

The purpose of this study is to examine methane, laminar gas-jet diffusion flames subjected to a coaxial, forced air flow by measuring flame shapes in the normal-gravity, zero-gravity, and inverted-gravity flame conditions. Air was forced through a convergent nozzle (coaxial with fuel nozzle) into a quiescent environment. In reference 11, experiments were performed with coaxial forced-air flow in a glass tube surrounding the flame. The work reported herein differs from that in reference 11 in that no use

was made of a surrounding glass tube. Methane was selected as a fuel gas in order to allow the study of zero-gravity extinguishment behavior on large nozzles. The experiments were conducted in a normal-gravity environment as well as in a drop-tower facility which provided 2.2 seconds of zero gravity. The fuel-nozzle radii were 0.051-, 0.185-, and 0.305-cm inside radius. Fuel flow rates ranged from 1.55 to 10.3 std cm^3/sec, while air flow rates ranged from 0 to 597 std cm^3/sec. Data are also presented on flame liftoff and blowout in normal-gravity and inverted-gravity conditions. A computer program developed under a previous government contract (ref. 7) was used as a basis for calculating diffusion-flame characteristic dimensions for the positive-gravity- and zero-gravity-level test results reported herein.

Symbols

a,b calibration constants

c_s methane mole fraction for stoichiometric burning with air, 0.095

E bridge voltage, V

L axial length of flame, cm

Q_a flow rate of air at nozzle exit under standard conditions, cm^3/sec

Q_f flow rate of methane fuel under standard conditions, cm^3/sec

R_M maximum radius of flame, cm

R_o inside radius of fuel nozzle, cm

R_p probe resistance, ohms

R_w outside radius of fuel nozzle, cm

Re_a air-flow Reynolds number, $R_w V_a/\nu_a$

Re_f fuel-flow Reynolds number, $R_o V_f/\nu_f$

Sc fuel Schmidt number (ratio of methane kinematic viscosity to diffusion coefficient), 0.744

V_a Free-stream axial velocity of air at nozzle exit, cm/sec

V_f average axial velocity of fuel at nozzle exit, cm/sec

δ_a thickness of boundary layer on air nozzle, cm

δ_f thickness of boundary layer on exterior surface of fuel nozzle, cm

ν_a kinematic viscosity of air at standard conditions, 0.1511 cm^2/sec

ν_f kinematic viscosity of methane at standard conditions, 0.1648 cm^2/sec

τ_a air time, R_w/V_a, msec

τ_f fuel time, R_o/V_f, msec

Apparatus and Procedures

Experiment Package

The experiment package was designed primarily for the zero-gravity tests. The zero-gravity tests were conducted at the Lewis Research Center's 2.2-Second Drop Tower Facility. Details on this facility and its operation are given in reference 10. A near weightless condition (termed "zero-gravity" in this report) of the order of 10^{-5} of Earth normal gravity was obtained by allowing the experiment package contained within an air-drag shield to free-fall a distance of 23 meters.

The experiment package is shown in figure 1. All of the equipment necessary for successful operation of the experiment was mounted on board this package. It contained a clock, camera, combustion chamber, methane and air-flow systems, carbon dioxide safety system, and associated direct-current power supplies and electronic controls. A high-speed (400 frames/sec), 16-mm motion-picture camera using Ektachrome EF (tungsten) film was used to photograph the flame and digital clock. Depending on the flame size, pictures were taken with either a 17- 25-, or 33-mm lens with an aperture setting of f2.8, f1.4, or f1.1, respectively. The aperture was open 39 percent of the running time. The film was processed to an ASA of 250. The digital clock was accurate to ±0.01 second. The combustion chamber was 41 by 41 by 48 cm in size. The top of the chamber had holes in it to prevent any pressure increase in the combustion chamber during burning. One wall of the chamber was made of clear plastic, so that the burning process could be photographed.

The various flow systems on board are shown in figure 2. The methane was stored at 1.5 MN/m^2 in a 500-ml vessel, air at 7.0 MN/m^2 in two 500-ml vessels. Regulators in the methane and air flow systems maintained the gas pressures downstream at 0.17 and 0.27 MN/m^2, respectively. Solenoid valves were used to start and stop the flow in the proper test sequence. Series-redundant solenoids were used on the methane system and parallel-redundant solenoids on the carbon dioxide system to provide fail-safe

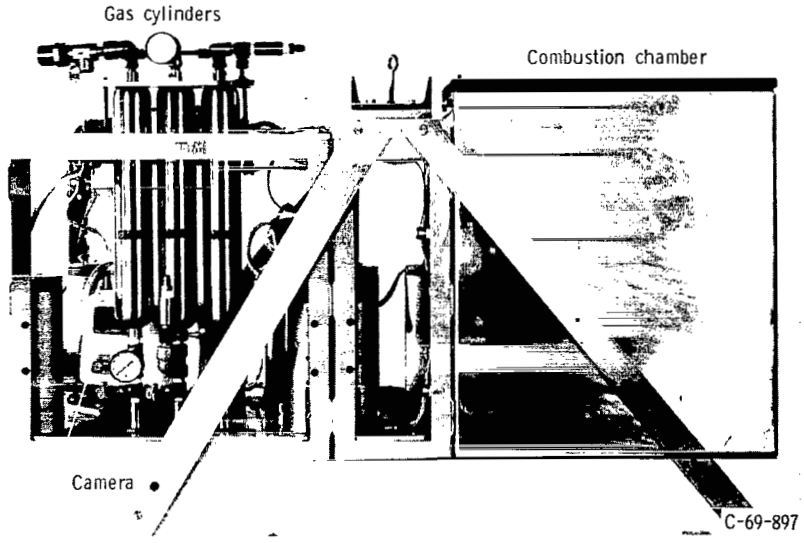

Figure 1. - Experiment package.

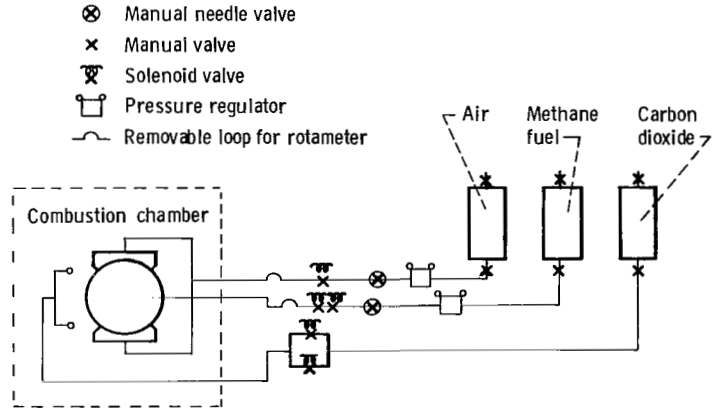

Figure 2. - Flow schematic for experiment.

protection to the experiment. The air and the methane systems both had manual needle valves to control gas flow, and both systems had removable sections so that calibrated rotameters could be placed in each system. The rotameters remained in the system during ground testing and were used to accurately measure the fuel and air flow rates. For the zero-gravity tests, the rotameters were used only to obtain preset positions for the needle valves. The rotameters were then removed from the systems prior to each zero-gravity test.

The carbon dioxide was delivered to the combustion chamber upon completion of the test to dilute its contents below the flammability limit. The methane and air was delivered to the test apparatus located within the combustion chamber as shown in figure 3. The methane flowed through a circular tube (nozzle) that was sufficiently long and straight to assure a parabolic velocity profile at the nozzle exit. The air was delivered through four tubes located 90° apart into an air chamber coaxially surrounding the fuel nozzle. Within the chamber, air flowed over and around two circular baffles before exiting through a convergent nozzle whose exit was coplanar with the fuel nozzle exit. The convergent nozzle, used to obtain a square velocity profile in the exiting air

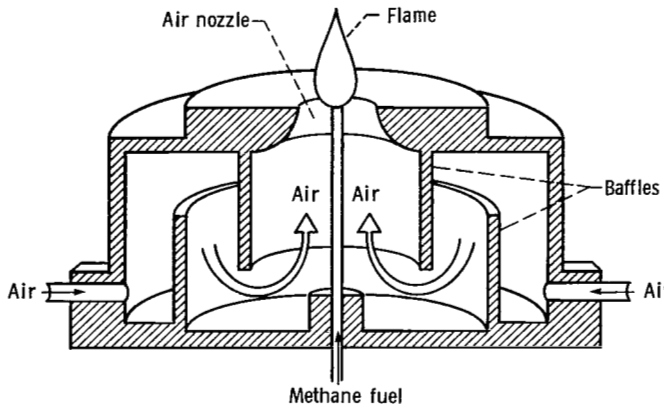

Figure 3. - Fuel-nozzle and air-chamber test apparatus.

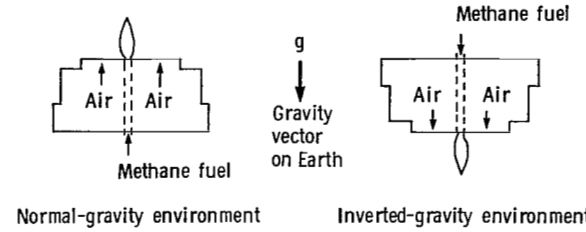

Figure 4. - Alignment of the gravity vector.

stream, had a circular contour of 1.4-cm radius. The geometry of the fuel-nozzle and air-chamber apparatus was such that it would produce a diffusion flame in an open, quiescent, air environment when the chamber air flow was zero.

A small Nichrome wire over the fuel nozzle was used to ignite the fuel. The three fuel nozzles used had inside radii of 0.051, 0.186, and 0.305 cm and outside radii of 0.081, 0.239, and 0.476 cm, respectively.

Ground-Test Procedures

Several series of ground tests were conducted to provide data for comparison with the zero-gravity test results. Two series were conducted on normal-gravity flames (1 g) and inverted-gravity flames (-1 g). Another series of ground tests were devoted to obtaining air velocities near the nozzle exit plane.

The orientation of the fuel and air nozzles with respect to Earth's gravity vector for both types of flames are displayed in figure 4. By placing the experiment package so that the forced fuel and air flow was directed vertically upwards, buoyancy acted to increase the local flow velocities, and a normal-gravity flame resulted. When the experiment package was placed so that the forced flow was directed vertically downward, buoyancy acted to inhibit local gas velocities, and an inverted-gravity flame resulted. Tests were conducted over a range of both fuel and air flow rates, the air flow rate being decreased to zero for some cases. These tests were accomplished by placing rotameters in the flow systems, establishing a flame, and adjusting needle valves in each system until the desired volumetric fuel and air flow rates were obtained. Once the experiment was on test condition, the camera and clock were started.

Another series of ground tests, devoted to obtaining air velocities, was accomplished with the use of a hot-film, constant-temperature anemometer. A stand with a movable mount for the probe, was constructed so that the centerline of the probe was allowed to move only radially towards or away from the fuel nozzle. The probe sensor axis was fixed perpendicular to the axis of the fuel nozzle and was maintained 0.23 cm above the exit plane. The probe had a quartz-coated, hot-film, cylindrical sensor 0.015 cm in diameter and 0.2 cm long and was operated at an overheat ratio of 1.3. Air flow tests were conducted with each of the three fuel nozzles. No methane was allowed to flow during these tests. For a given fuel nozzle, air flow, and radial station, the change in heat dissipated at the probe sensor was detected and related to the flow velocity by a method to be described later.

Drop-Tower Test Procedure

In preparation for a zero-gravity test, the experiment-package supply bottles were filled with methane, air, and carbon dioxide, as required. The rotameters were installed, and the methane and air flows were started. By adjusting the manual needle valves, the desired volumetric flow rates were obtained. The flows were stopped by closing the solenoid valves in each system, and the rotameters were removed. An igniter wire was suspended near the fuel nozzle. The experiment package was placed in the air drag shield, and this entire assembly was suspended from the top of the drop tower.

The zero-gravity tests began when the camera and clock were switched on. The methane flow was also started by activating the appropriate solenoid valves. Two seconds later, current was delivered to the igniter wire, and a flame was initiated. One second after ignition, the air flow was started by activating

the appropriate solenoid valves. The entire system was then allowed to come to a steady-state condition over a period of about 3 seconds. The zero-gravity condition was then imposed by allowing the experiment package and air drag shield to free-fall. Upon completion of the fall, the camera, clock, and air and methane flows were switched off, and the carbon dioxide purge of the combustion chamber was effected.

Data Reduction

Flame length and width measurements as a function of time, as well as general observations, were made by viewing the motion-picture film of the tests. The measurements were made with the aid of a motion-picture analyzer, which enlarged the film image 24 times and used crosshairs to measure lengths to within ± 0.003 cm on the enlarged image. The ratios of measured length to actual length were obtained by photographing a scale which had 0.1-cm divisions and was mounted above the nozzle. This was done for each lens that was used.

Results and Discussion

Hot-Film Anemometer Tests

A series of ground tests were conducted with the use of a hot-film anemometer to ascertain the air flow velocity profile near the exit plane of the air-flow nozzle. The importance of these tests cannot be stressed too greatly inasmuch as any complete analysis of the behavior of a gas-jet diffusion flame requires a complete description of the boundary conditions in the region of interest.

The hot-film constant-temperature anemometer tests used a probe with a quartz-coated, hot-film, cylindrical, 0.015-cm-diameter by 0.2-cm-long sensor; a root-mean-square (rms) voltmeter; a probe mount and support stand; and an accurate dial-indicator gauge. The probe in its movable mount was positioned in its support stand at a height nearly coincident with the exit plane of the air nozzle (0.23 cm above the nozzle exit), and along a radius emanating from the principal axis of the air nozzle. The probe was positioned so that the axis of the sensor was perpendicular to the flow direction. The output of the constant-temperature anemometer was connected to the rms voltmeter and was filtered with a 10-kHz low-band pass filter to eliminate extraneous, high-frequency noise. During the testing, the volumetric air flow rate was measured with a calibrated rotameter. For these tests, the fuel flow was never turned on.

For a given volumetric air flow rate, the bridge voltage of the anemometer and the rms voltage were read at a series of radial stations. If E is the bridge voltage, R_p is the known probe sensor resistance, and V is the axial air velocity at a given station, then by King's equation (ref. 12), $E^2 R_p/(R_p+40)^2 = a+bV^{1/2}$, where a and b are constants to be determined by an independent calibration procedure. Such calibration procedures were not used, primarily because of the difficulty of obtaining a known low-velocity air stream. Instead, it was observed that the measured bridge voltage was constant, hence the velocity was constant, except in the boundary layers at the exterior wall of the fuel nozzle and the interior wall of the air nozzle. Therefore, these tests were used only to determine the boundary-layer thicknesses. The velocity profile in the boundary layer was assumed to be parabolic in shape. With this assumption, and the measured volumetric air flow rate, the free-stream air velocity was calculated from the following equation:

$$V_a = \frac{Q_a}{\pi\left[1.4^2 - 0.933\delta_a + (1/6)\delta_a^2 - R_w^2 - (2/3)\delta_f R_w - (1/6)\delta_f^2\right]} \tag{1}$$

Seventeen test runs were made with the three fuel nozzles used in this study, and with the air flow rate varied from 10 to 765 cm^3/sec. The results are presented in figures 5 and 6.

Figure 5 presents the boundary-layer thicknesses experimentally found as a function of the volumetric air flow rate. To confirm these experimental results analytically, a computer program, GENMIX (ref. 13), was used. The curves shown in figure 5 present the results of the computer simulation at the same test conditions. As can be seen in the figure, the computer results and the experimental data match quite well. These data imply that the intent of the design of the air nozzle, which was to approximate an air flow condition in which the velocity profile was

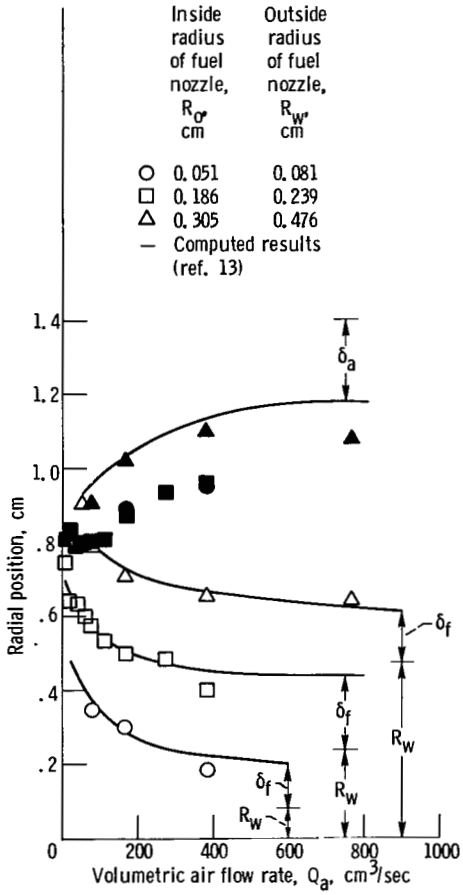

Figure 5. - Comparison of computed and experimentally determined boundary-layer thicknesses near the fuel exit plane in the annular air-flow region.

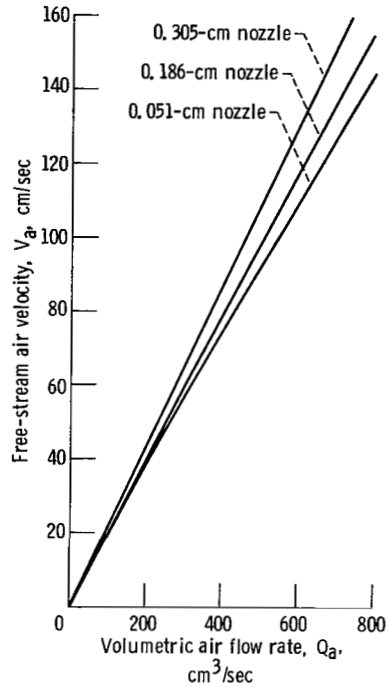

Figure 6. - Dependence of free-stream air velocity on volumetric air flow rate near the fuel exit plane.

flat in the radial direction, had been achieved. The boundary layer on the fuel nozzle was always of the order of magnitude of R_o, the inside nozzle radius; hence, the influence of this boundary layer on the flame geometry and structure must unavoidably be considered. Above an air flow rate of 100 cm^3/sec, the boundary layer on the interior wall of the air nozzle can be seen to be very small.

The hot-film tests demonstrated that the air flow velocity in the free stream outside the boundary layers was substantially constant. Figure 6 presents plots of the computed free-stream velocity as a function of volumetric flow rate. Three curves are given for the three fuel nozzles used in the study. It should be noted that these curves, because of the presence of the boundary layers, yield substantially higher free-stream velocities than the average velocities calculated from the ratio of volumetric air flow rate to the cross sectional area of the air nozzle.

Ground Tests Without Forced Air

This series of ground tests was conducted by allowing only methane flow and was used to determine the effects of axial flame length and maximum flame radius on volumetric flow rate for both normal-gravity and inverted-gravity flames. The resulting data are shown in figures 7 and 8. From the data in figure 7(a), it was found that the axial length of the normal flames is nearly linearly dependent on the fuel volumetric flow rate. There was a very weak effect of nozzle radius on the data. While the inverted-gravity flame lengths shown in figure 7(b) also displayed a linear dependence on volumetric flow rate, there appeared to be a strong dependence on the nozzle radius. The axial flame length measurements indicate that the normal-gravity flames were always longer than the inverted-gravity flames at the same test conditions. The axial length of the inverted-gravity flames ranged from 15 percent shorter, on the 0.051-cm-radius nozzle, to 85 percent shorter, on the 0.305-cm-radius nozzle, as compared

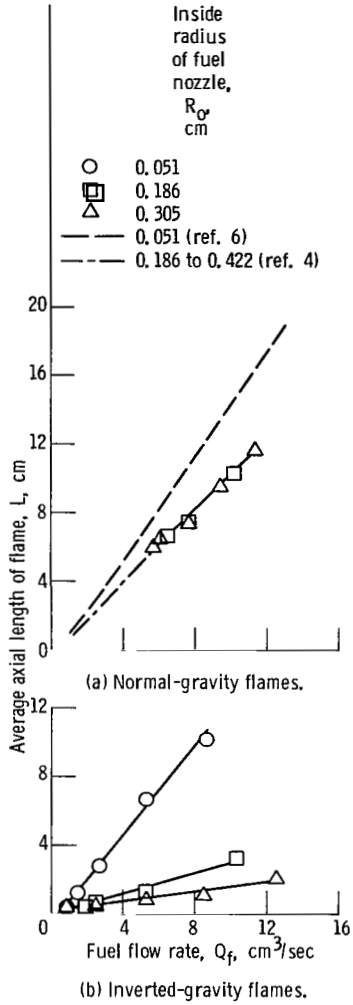

Figure 7. - Average axial length of normal-gravity and inverted-gravity flames without forced air flow.

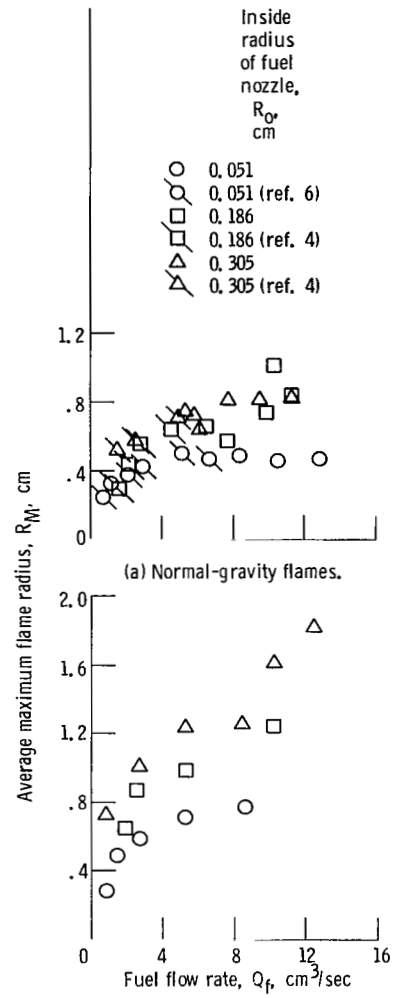

Figure 8. - Average maximum radius of normal-gravity and inverted-gravity flames without forced air flow.

to the corresponding normal-gravity flames.

It is worth noting that the axial flame length measurements made in zero gravity (ref. 10) indicate that, for those conditions where steady-state flames existed, the zero-gravity flames were 50 percent longer than their normal-gravity counterparts. The fact that the zero-gravity data do not fall between the normal-gravity data and the inverted-gravity data indicates the complicated role gravity plays in this process.

Data on the maximum radius for both normal-gravity and inverted-gravity flames are presented in figures 8(a) and 8(b). For both types of flame, the maximum flame radius increased as the volumetric flow rate increased. The maximum radii of normal-gravity flames had a slight parametric dependence on nozzle radius (i.e., increasing maximum radius for increasing nozzle size). The maximum radius for inverted-gravity flames showed a considerably stronger dependence on nozzle size. At the same volumetric flow rate, the maximum radius was always greater for inverted-gravity flames than for normal-gravity flames—approximately 40 percent greater for the 0.051-cm-radius nozzle, and 70 percent greater for the 0.305-cm radius nozzle.

The zero-gravity, steady-state, maximum-radius data (ref. 10) for the 0.051-cm-radius nozzle indicate that zero-gravity flame radii are greater than either

normal-gravity or inverted-gravity flame radii. The zero-gravity flames were about 50 percent wider than their normal-gravity counterparts.

For these tests without forced air flow, some observations may be made concerning the role of buoyancy in determining flame geometry. Buoyancy acts to accelerate the flow for normal-gravity flames. This accelerated flow can inhibit the spread of the fuel in the radial direction, thus causing the flame to lie near the jet axis. Conversely, buoyancy decelerates the flow for inverted-gravity flames to the point that backflow or recirculation may occur. The radial spread of the jet would, therefore, be widened over that found in normal-gravity flames. Hence, we would expect normal-gravity flames to be thin and long, and inverted-gravity flames to be short and wide. A surface where stoichiometric conditions exist probably occurs in the flame zones of both flames because of their good fuel-oxidant mixing characteristics. In contrast, zero-gravity flames have been observed to not have good mixing characteristics. They produce large amounts of soot and possess colors within longer wavelength regions (ref. 10). These observations would indicate that the flame zone is burning fuel-rich at lowered flame temperatures. Apparently, the absence of buoyancy decreases the delivery of oxidant to, and removal of products from, the flame zone. In the absence of buoyancy, diffusion is the principal process operating to mix the fuel and oxidant. Therefore, the fuel must travel further, both radially and axially, in order to reach oxidant so that there is an acceptable fuel/oxidant ratio for combustion to occur. This interpretation would possibly explain why zero-gravity flames are both longer and wider than normal-gravity flames or inverted-gravity flames.

In reference 10, a correlation has been found for the maximum-flame-radius data without air flow in normal gravity and zero gravity. It was found by a computer analysis (ref. 7) that the ratio of the maximum flame radius to the nozzle radius was proportional to the common logarithm of the fuel time ($\tau_f = R_o / V_f$) by the following relations:

For normal-gravity flames,

$$R_M/R_o = 5.75 - 3.7 \log \tau_f \qquad (2)$$

For zero-gravity flames,

$$R_M/R_o = 10.5 - 3.7 \log \tau_f \qquad (3)$$

Comparison of the normal-gravity flame data of this report with equation (2) is shown in figure 9. As can be seen, the agreement is excellent.

When the inverted-gravity, maximum-flame-radius data were nondimensionalized with respect to the nozzle radius and plotted against the log τ_f, also shown in figure 7, the best fit to the data was given by

$$R_M/R_o = 8.55 - 3.7 \log \tau_f \qquad (4)$$

It should be noted in figure 9 that the nondimensionalized maximum flame radius ceases to be proportional to the log τ_f for τ_f greater than 5 to 10 milliseconds. Of primary importance, however, is that a correlation has been developed that matches the experimental data to within an empirically determined constant that is dependent on the local gravity field. This relationship is valid for radically different flow situations over better than two orders of magnitude in the fuel time.

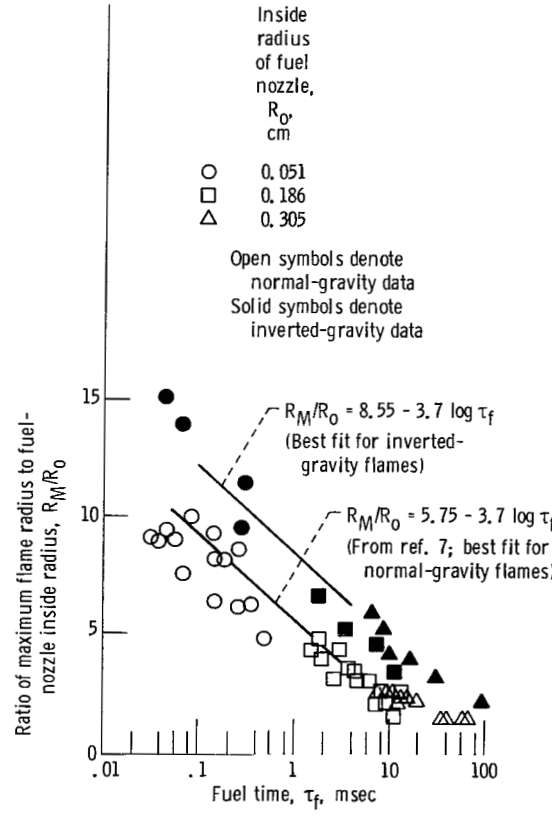

Figure 9. - Correlation of normalized maximum radius of normal-gravity and inverted-gravity flames with fuel time, without forced air flow.

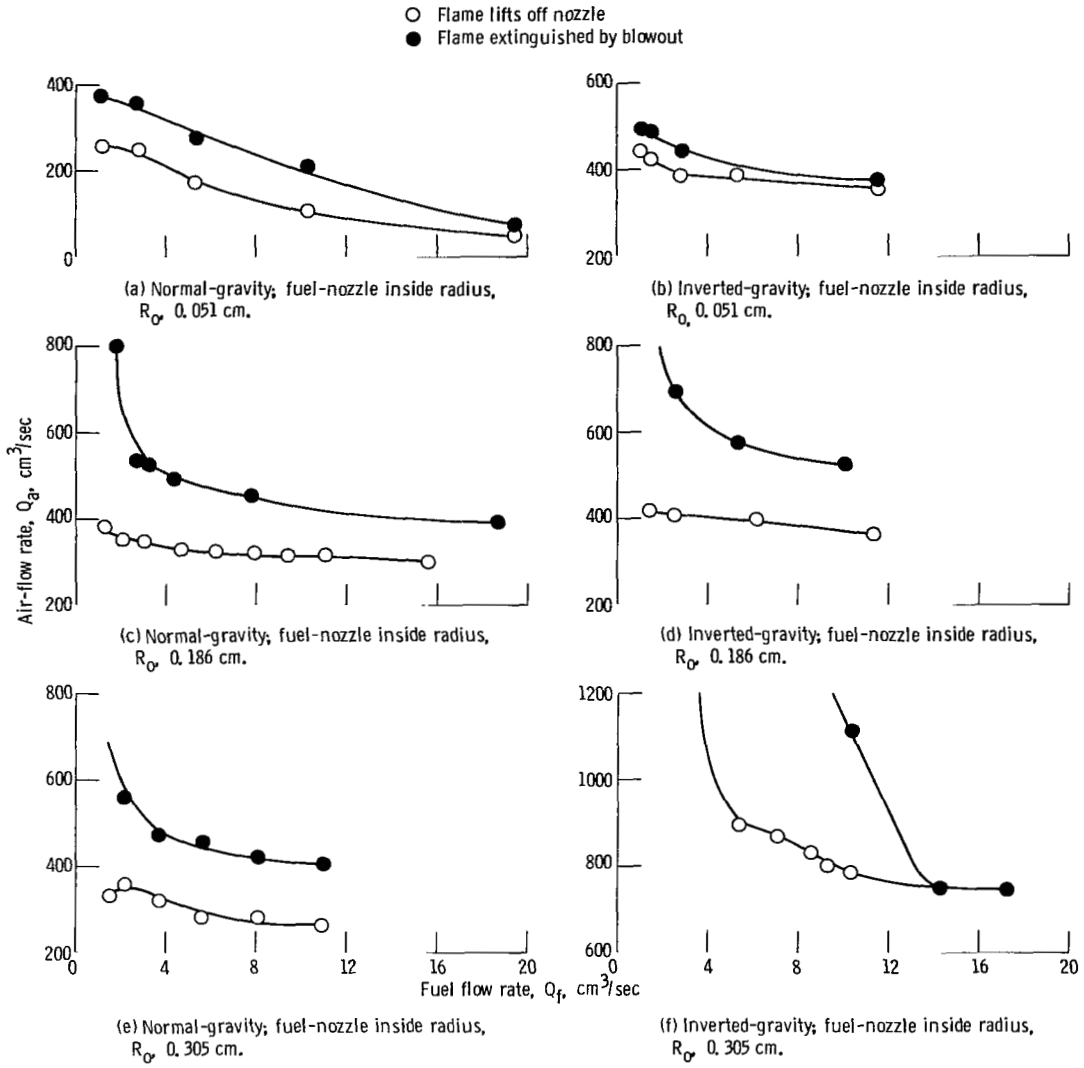

Figure 10. - Lift and blowout curves for normal-gravity and inverted-gravity flames.

Lift- and Blowout-Limit Tests With Forced Air

A series of ground tests was conducted with normal-gravity and inverted-gravity flames with coaxial forced air flow in order to determine the extent of the air flow domain over which a diffusion flame could be stabilized anywhere in the flow field. Two stable configurations exist for this combustion phenomenon—flames attached to the nozzle rim, and flames stabilized at some distance away from the nozzle exit plane. The lifted flame limit, which is defined as that condition wherein any increase in either the fuel flow or the air flow will cause an attached flame to rise off the nozzle, separates these two regions. The blowout limit separates stabilized lifted flames from the unstable situation wherein a flame propagates continually downstream to extinction.

Figure 10 presents the lift and blowout limits for normal-gravity and inverted-gravity flames on the three nozzles tested. Several general trends can be seen with these data. The higher the fuel flow rate for a given nozzle, the lower the air flow required to both lift and blow out the flame. Also, generally for a given fuel flow rate, lower air flow rates were required to both lift and blow out flames as nozzle size decreases. Lift and blow-out limits for inverted-gravity flames generally occurred at higher air flow rates than for normal-gravity flames.

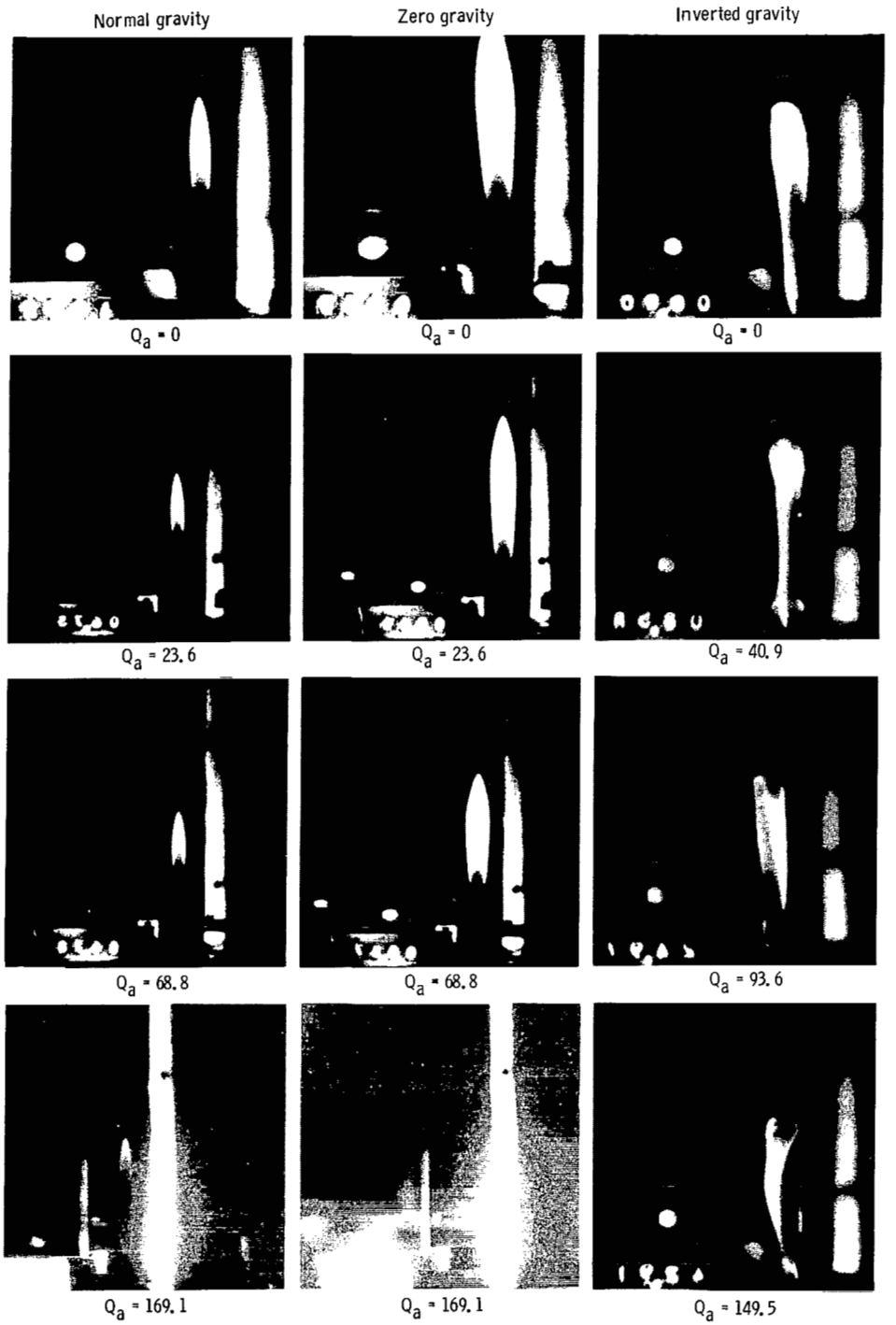

(a) Fuel-nozzle inside radius, R_0, 0.051 cm.

Figure 11. - Normal-gravity, steady-state zero-gravity, and inverted-gravity flames with three sizes of fuel nozzle, at a fuel flow rate, Q_f, of 5.3 cm^3/sec, and at various air flow rates, Q_a (given in cm^3/sec).

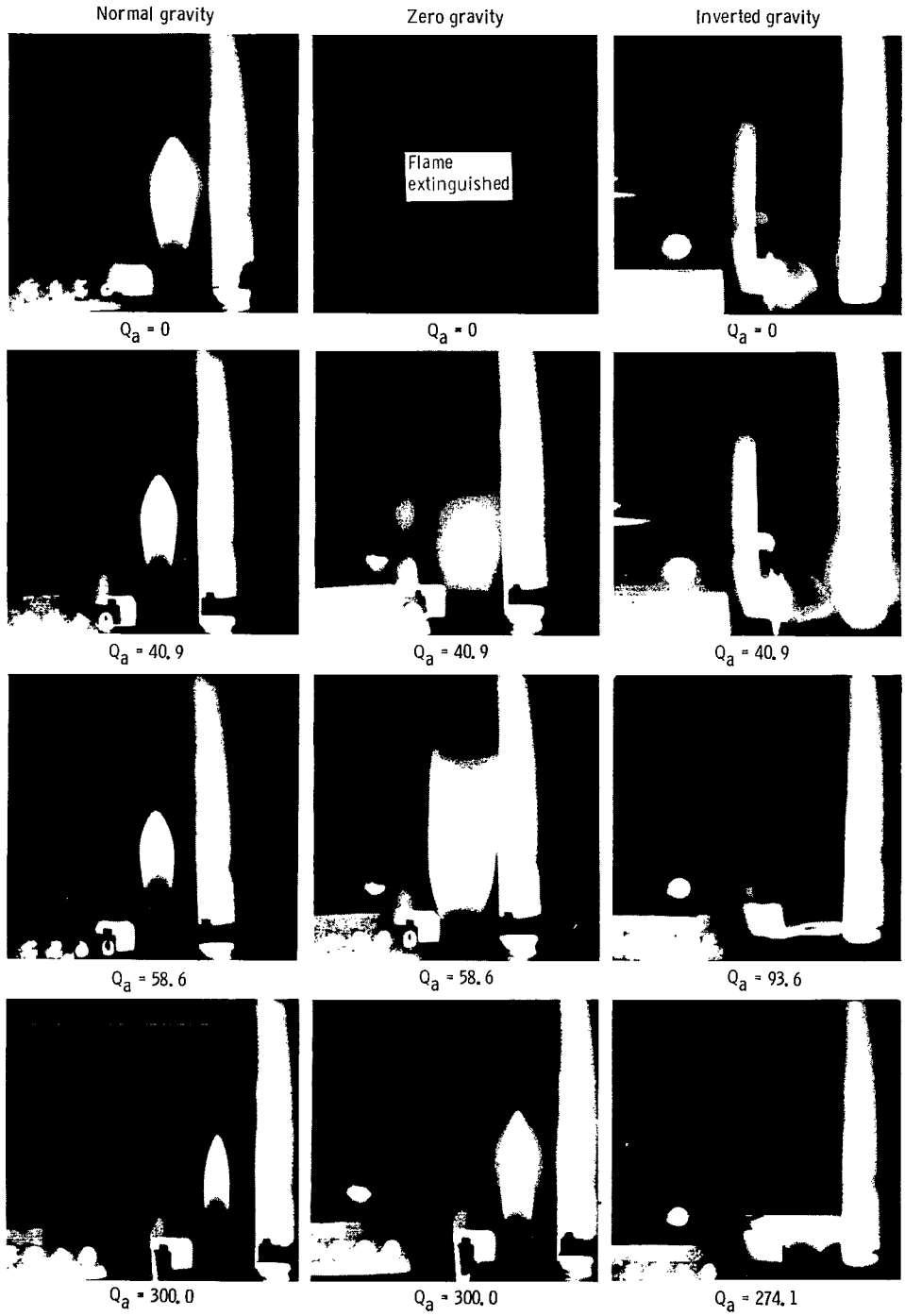

(b) Fuel-nozzle inside radius, R_o, 0.186 cm.

Figure 11. - Continued.

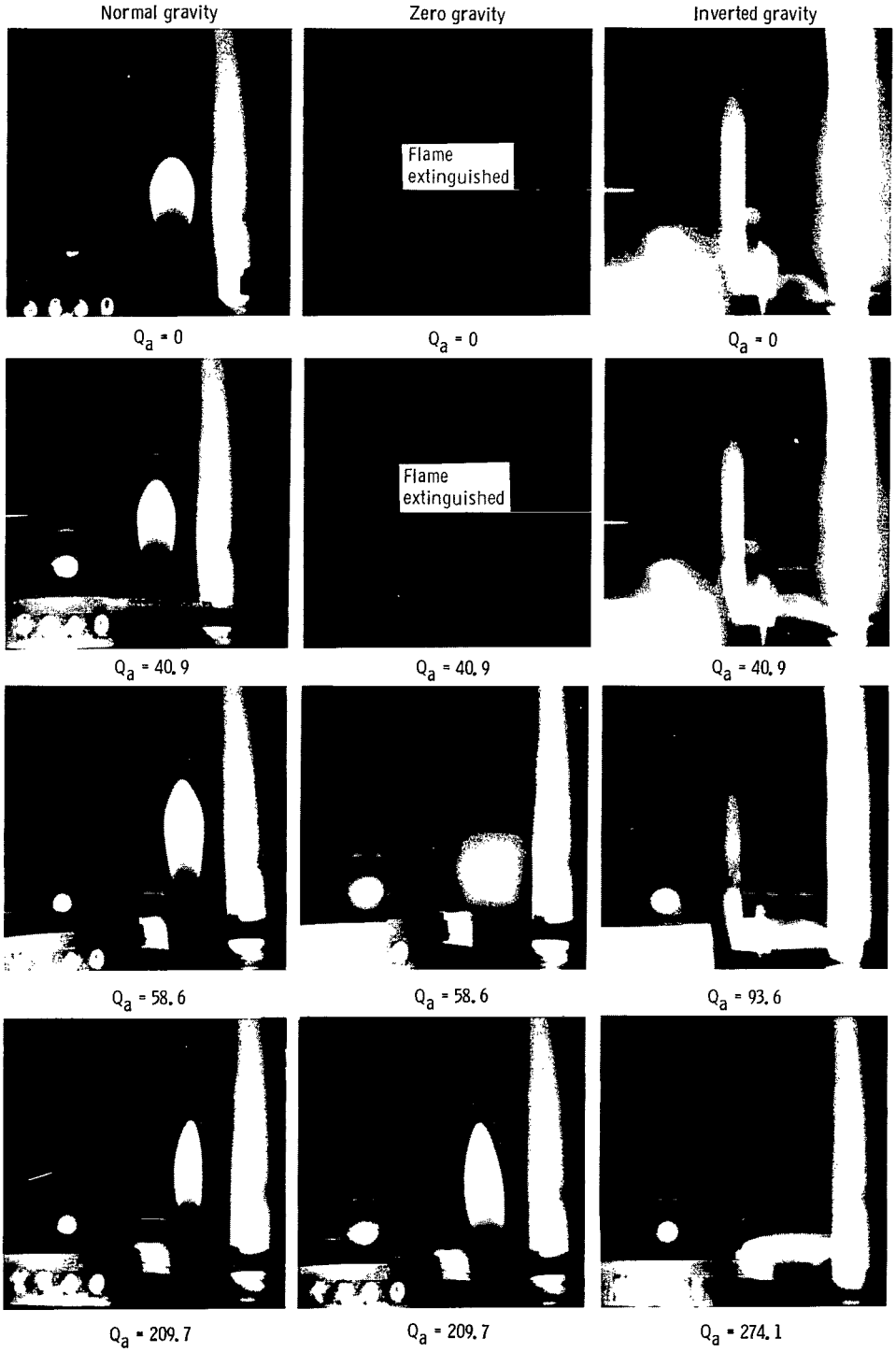

(c) Fuel-nozzle inside radius, R_o, 0.305 cm.

Figure 11. - Concluded.

Drop-Tower and Ground Tests With Forced Air Flow

All of the data obtained with forced flow on zero-gravity, normal-gravity, and inverted-gravity flames are presented for convenience in tables I to III. Data were taken for each of the three nozzles at three different fuel flow rates and at four to ten different air flow rates per configuration. Both the axial length and the maximum radius were measured for each flame.

Figure 11 presents some of the photographs taken of normal-gravity, zero-gravity, and inverted-gravity flames. In all of the photographs, the fuel flow rate was 5.3 ± 0.1 cm^3/sec. The reader is cautioned that some of the photographs were taken with different lenses so that the enlargement of the flame may be different. Each photograph contains a flame against a black background, a digital clock in the lower left corner of the picture, and a light box as a source of illumination.

For the smallest fuel nozzle (0.051 cm radius), a steady-state, zero-gravity flame was found to exist when there was no air flow. Further, the zero-gravity and the normal-gravity flames appeared similar in shape, although the zero-gravity flame was larger, both radially and axially. This general behavior was true for all tests in which there was a coaxial air flow with this size nozzle. At the highest air flow rate of 169.1 cm^3/sec, both the normal-gravity and zero-gravity flames were faint and blue in appearance. However, the zero-gravity flame was lifted off the nozzle. The inverted-gravity flames were significantly different in appearance from the corresponding normal-gravity and zero-gravity flames. These inverted-gravity flames had a ball-like shape at their top. In addition, they appeared more unstable, twisting back and forth on the nozzle.

For the 0.186-cm-radius nozzle, no zero-gravity flame was found to exist for zero air flow. For the zero-gravity test at an air flow rate of 40.9 cm^3/sec, a faint orange, steady flame was stabilized on the nozzle. In zero gravity at air flow rates of 40.9 and 58.6 cm^3/sec, the zero-gravity flame was an open-topped, underventilated flame in contrast to the closed-topped, overventilated flame that appeared in normal gravity. At the highest air flow rate, both the normal-gravity and zero-gravity flames appeared overventilated. However, the zero-gravity flame was still larger than the normal-gravity flame. The inverted-gravity flames at low air flow rates had an egg-shaped appearance, strikingly different from the inverted-gravity flames on the smaller, 0.051-cm-radius nozzle. At an air flow rate of 93.6 cm^3/sec, the flame appears almost disk shaped. Finally, at the highest air flow rate, the inverted-gravity flame has an anvil-like appearance.

For the 0.305-cm-radius nozzle, there again was no zero-gravity flame until the air flow rate reached 58.6 cm^3/sec, where a faint, underventilated flame appeared stabilized. At the highest air flow rates, the zero-gravity and normal-gravity flames were similar in appearance—overventilated, with the zero-gravity flame being larger. The inverted-gravity flame behaved similarly to its behavior on the 0.186-cm-radius nozzle.

Before examining the normal-gravity, zero-gravity, and inverted-gravity flame data with forced air flow, a discussion of the behavior of a typical diffusion flame upon entry into zero-gravity is necessary. Figure 12 presents plots of axial length versus zero-gravity time for diffusion flames from two different test runs, each burning on the same nozzle (0.186 cm radius), at the same fuel flow rate (2.71 cm^3/sec), without forced air flow. The only physical difference between the two tests was that in one case (fig. 12(a)), the air chamber surrounding the fuel nozzle was in place, while in the second instance (fig. 12(b)), the fuel nozzle stood off the combustion-chamber floor in a manner similar to test configurations reported in references 4, 6, and 10. Before entering zero gravity, both flames had a mean axial length of 2.68 cm, and both were flickering. Upon entry into zero gravity, for the test conducted with no air chamber (fig. 12(b)), the flame behaved in a manner similar to other extinguished zero-gravity flames; that is, there was at first a sharp reduction in the axial length, followed by a gradual expansion of the flame front away from the nozzle until the flame was extinguished 0.63 second after entry into weightlessness. The test conducted with the air chamber surrounding the nozzle (fig. 12(a)) also resulted in the flame being extinguished. However, the manner in which it was extinguished was entirely different. Upon entry into weightlessness, the flame underwent several rapid oscillations during which the flame seemed to almost disappear. Following the oscillations, the flame did not appear to expand away from the nozzle but rather it gradually faded in color until it was extinguished at 0.92 second. Because of the manner in which these two flames were

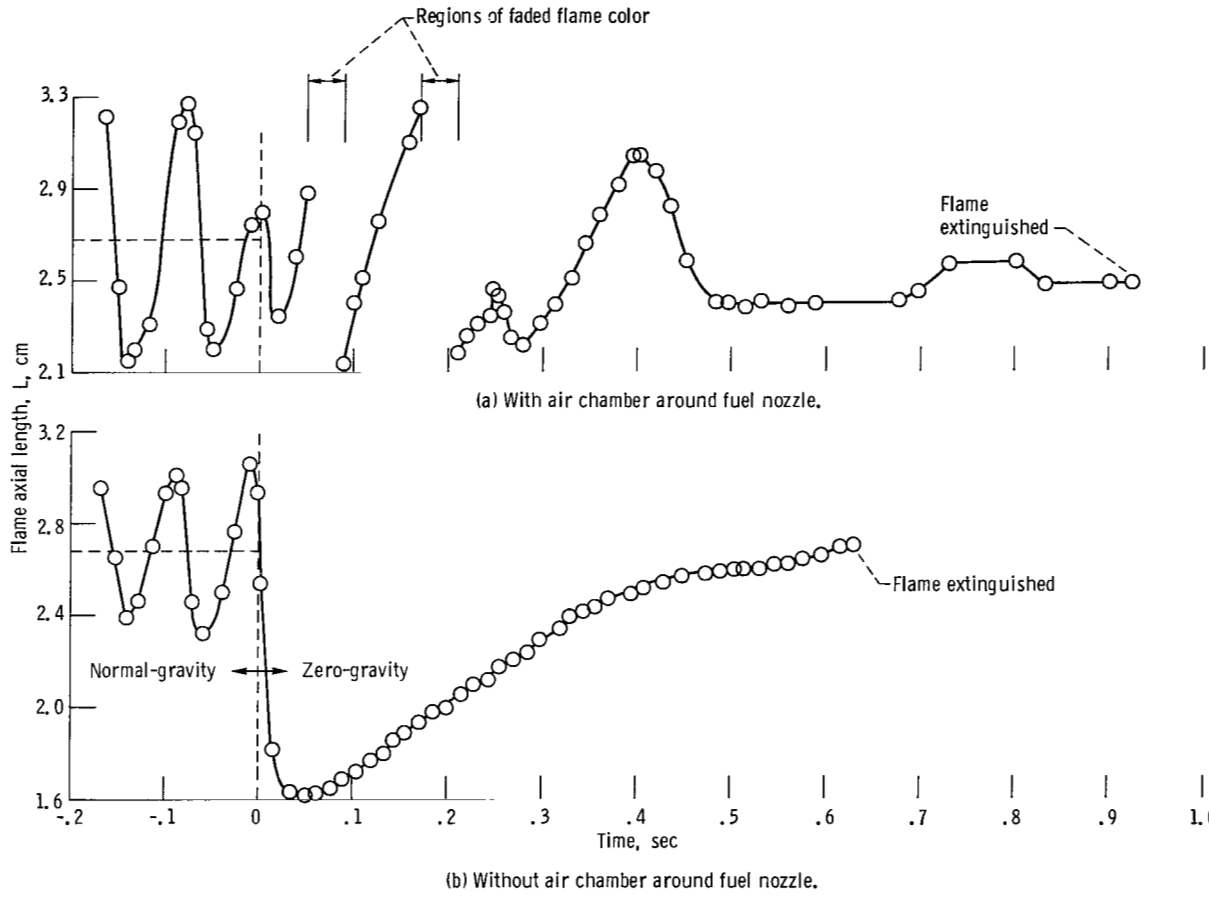

Figure 12. - Typical time profiles of axial flame length upon entry into weightlessness, with and without air chamber around fuel nozzle. Fuel-nozzle inside radius, R_o, 0.186 cm; fuel flow rate, Q_f, 2.71 cm^3/sec; air flow rate, Q_a, zero.

extinguished, it may be inferred that the aerodynamics of the air flow surrounding the flame, particularly at its base, play a substantial role in determining the manner in which zero-gravity flames are extinguished in drop-tower testing.

Figure 13 presents the correlation of the normalized axial flame length with the air flow Reynolds number for the zero-gravity test results. Consider first the cases where the air flow Reynolds number is zero. In reference 9, zero-gravity axial flame length for a variety of hydrocarbon fuels was correlated for flames with no forced air flow by the equation

$$L/R_o = 3.5\, Sc^{1/2} Re_f \ln^{1/2}\left[1/(1-c_s)\right] \qquad (5)$$

where the fuel Schmidt number (Sc) is the ratio of kinematic viscosity to diffusion coefficient, and c_s is the fuel mole fraction for stoichiometric burning. All the physical constants are evaluated at room temperature. For the test fuel, methane, $Sc = 0.744$, $c_s = 0.095$, and $\nu_f = 0.1648$ cm^2/sec. Therefore, $3.5\, Sc^{1/2} \ln(1/(1-c_s))$ is equal to 0.97, and without forced air flow, the zero-gravity flame length is

$$L/(Re_f R_o) = 0.97 \qquad (6)$$

Consider now the coaxial forced air flow situations. It is reasonable to assume that the Reynolds number of the air flow ($Re_a = R_w V_a/\nu_a$) with fluid properties evaluated at 20° C and 1 atm, the fuel-nozzle outside radius (R_w), and the free-

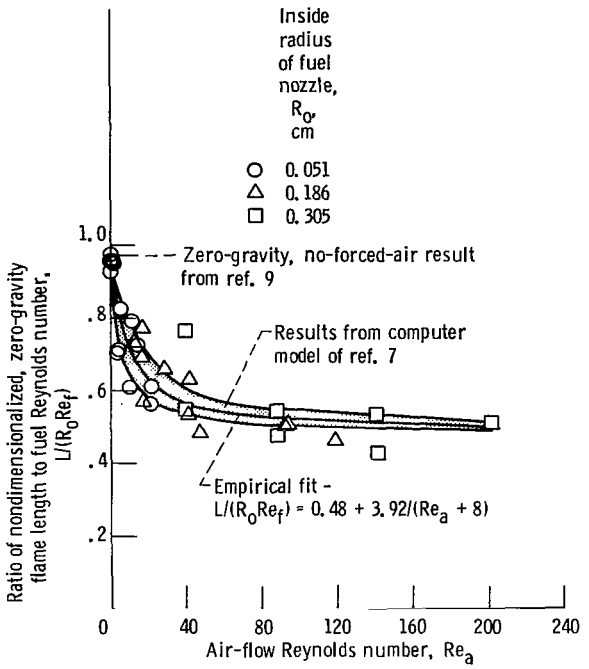

Figure 13. - Correlation of normalized axial flame length with air-flow Reynolds number for zero-gravity flames.

stream air velocity (V_a) would characterize the forced convection effects. The kinematic viscosity of the air was taken to be 0.1511 cm^2/sec. Accordingly, in figure 13, $L/Re_f R_o$ (the ratio of nondimensional flame length to fuel Reynolds number) is plotted versus the air-flow Reynolds number for the majority of zero-gravity test conditions studied. It should be noted that three runs (#31, #49, and #50), besides those for which the flame was extinguished, were not plotted on this figure. The results of these runs fell well below the plotted data points with similar air-flow Reynolds numbers. These points occurred at the highest fuel flow rates and the lowest air flow rates for the two largest nozzles. A computation of the ratio of air flow to fuel flow revealed that an insufficient amount of air was being supplied for complete combustion. Hence, these flames were underventilated, or oxygen-starved.

It can be seen in figure 13 that the ratio of nondimensional length to Reynolds number falls quickly from about 0.97 at $Re_a = 0$, to about 0.58 at $Re_a = 30$, and gradually changes thereafter so that it is about 0.5 at $Re_a = 200$. The data were compared on a point-for-point basis to a computer model (ref. 7). The program solved the parabolic form of the equation of motion in addition to the continuity and energy equations. Both fuel and air flow were accounted for in the model. The chemistry assumed was a quasiglobal reaction scheme. The results of the computer model analysis are given as a cross-hatched region in figure 13. Instead of plotting the computer model results for each test run, it was decided, for simplicity of presentation, to consider the computer results collectively as comprising a region which could then easily be compared to the experimental data points. The computer-model results are considered to be in excellent agreement with the data. On the average, the computer results were within 1.3 percent of the experimental data. For practical purposes, the best empirical fit to the zero-gravity data with forced air flow is given by

$$L/(Re_f R_o) = 0.48 + 3.92/(Re_a + 8) \qquad (7)$$

Figure 14 presents the normal-gravity, axial-flame-length experimental results correlated with the air-flow Reynolds number in a manner similar to that

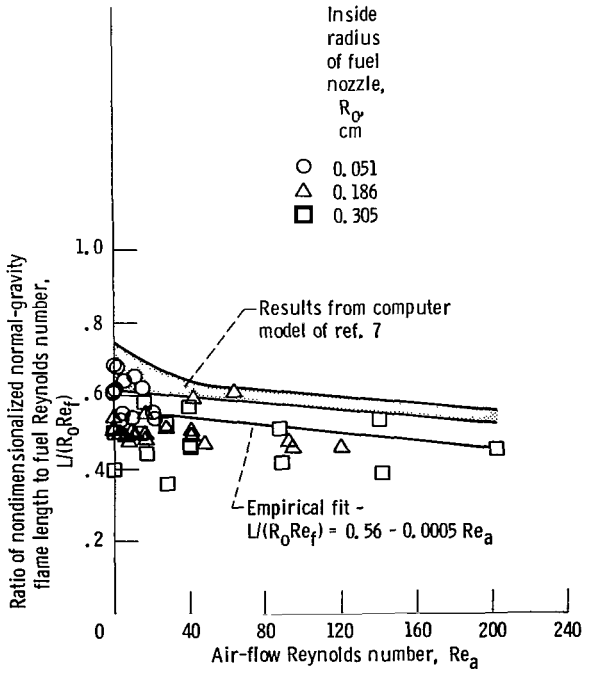

Figure 14. - Correlation of normalized axial flame length with air-flow Reynolds number for normal-gravity flames.

used for the zero-gravity results. It is recognized, however, that normal-gravity flames should not be correlated at small air-flow Reynolds numbers by this technique because of the presence of buoyancy forces which are not accounted for in this scheme. Nevertheless, buoyancy effects should be overcome at some point by the inertial forces of the coaxially flowing air stream, so that a correlating scheme similar to that used for zero-gravity flames should be valid at high air-flow Reynolds numbers. Some evidence of buoyancy effects on normal-gravity flame length for $Re_a = 0$ can be seen in figure 7(a) where the data are scattered, suggesting the importance of some other parameter. In figure 14, at high air-flow Reynolds numbers, some semblance of a correlation appears to be emerging. Although the computer-model analysis shown by the cross-hatched region rather consistently predictly higher ratios of nondimensional length to fuel Reynolds number than observed, it is of interest to note the trend of the predictions in terms of air-flow Reynolds number was similar to the actual data. The best empirical fit to the normal-gravity data with forced air flow data was found to be given by

$$L/(R_o Re_f) = 0.56 - 0.0005\ Re_a \qquad (8)$$

The air-flow Reynolds number range over which buoyancy effects are important in axial flame-length measurements may be determined by qualitatively comparing figures 13 and 14. The zero-gravity and normal-gravity results become reasonably close to one another at air-flow Reynolds numbers beyond about 40. Hence buoyancy effects in the flow situations tested are considered to be important if $Re_a \leq 40$.

Because of the complications of both buoyancy and recirculation flows within inverted-gravity flames, these data, when plotted in a manner similar to the zero-gravity and normal-gravity data shown in figures 13 and 14, failed to produce a consistent correlation over the entire air-flow Reynolds number range studied.

Consider now the zero-gravity, maximum-flame-radius data presented in figure 15. For the case of no air flow, it has been found in a prior study (ref. 9) that the ratio of maximum flame radius to nozzle radius could be correlated to the fuel time $(\tau_f R_o / V_f)$, in milliseconds, by the following equations:

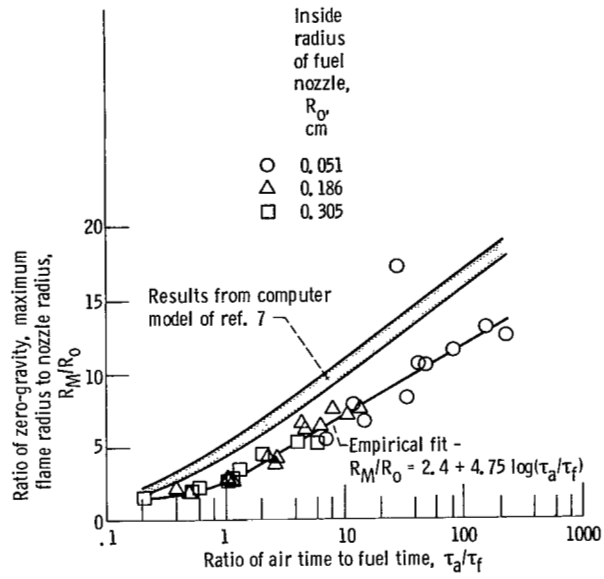

Figure 15. - Correlation of normalized flame radius with the ratio of air time to fuel time for zero-gravity flames.

For zero gravity,

$$R_M/R_o = 10.5 - 3.7 \log (R_o 1000/V_f) \qquad (9)$$

For normal gravity,

$$R_M/R_o = 5.75 - 3.7 \log (R_o 1000/V_f) \qquad (10)$$

The ratio R_o/V_f has units of time, and the ratio R_M/R_o is dimensionless. From this consideration, a correlation scheme for forced air flow situations was sought which would be appropriate and nondimensional. That correlating variable was found to be the ratio of air time to fuel time $(\tau_a/\tau_f = R_W V_f / R_o V_a)$. In figure 15, R_M/R_o is plotted versus the common logarithm of τ_a/τ_f. For characteristic time ratios of about 0.1, the nondimensional flame radius appears to approach the asymptotic limit of 1. In the characteristic time ratio range of 1 to 200, the best empirical fit to the data is given by

$$R_M/R_o = 2.4 + 4.75 \log(\tau_a/\tau_f) \qquad (11)$$

For small free-stream air flow velocities relative to the average fuel velocity and/or for excessively thick-

walled tubes relative to the inside nozzle radius, the ratio τ_a/τ_f is large. Under these conditions, air entrainment due to aspiration by the fuel flow is an important effect. This effect is unaccounted for in the present correlating scheme. Hence, it is expected that at some large value of τ_a/τ_f, the correlation given by equation (11) should fail. The data suggest that this characteristic time ratio is greater than 200. The test data in figure 15 were compared to the results given by the computer model of reference 7. The computer-model results, shown as a cross-hatched region in the figure, consistently predicted larger nondimensional flame radii ratios than observed, with an average error of 55 percent.

Figure 16 presents the correlated normal-gravity, maximum-flame-radius results. The same correlating scheme was applied to the normal-gravity, maximum-flame-radius data as was applied to the corresponding zero-gravity data in figure 15. The nondimensional flame-radius data were plotted versus the common logarithm of τ_a/τ_f. For characteristic time ratios of about 0.1, the nondimensional normal-gravity flame radius was again approaching an asymptotic limit of 1.

In the characteristic time-ratio range of 1 to 200, the best empirical fit to the data is given by

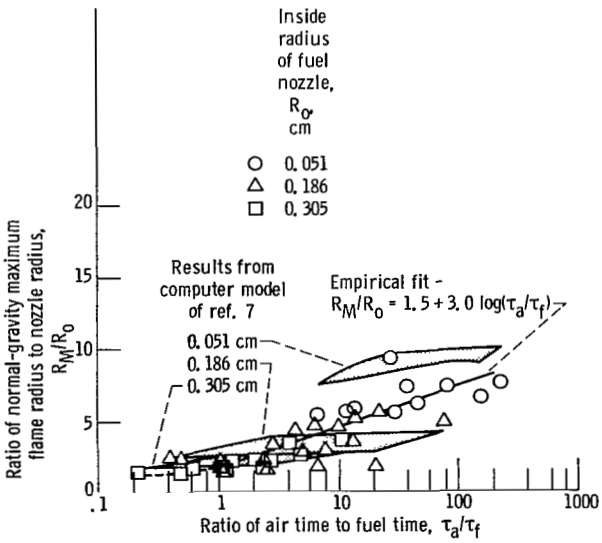

Figure 16. - Correlation of normalized flame radius with the ratio of air time to fuel time for normal-gravity flames.

$$R_M/R_o = 1.5 + 3.0 \log(\tau_a/\tau_f) \qquad (12)$$

The same comments made earlier regarding air entrainment induced by the fuel flow at large characteristic time ratios are applicable to the normal-gravity data. Additionally, buoyancy-induced air entrainment is important at large time ratios.

The results given by the computer model of reference 7, shown as cross-hatched regions in figure 16, display a rather strong fuel-nozzle-radius effect not found in any of the other computer results for normal-gravity and zero-gravity flames. The computer results for the 0.051-cm nozzle were consistently higher than data experimentally observed; the 0.186-cm results were slightly lower, and the 0.305-cm-nozzle results were about right. These results may be anticipated if buoyancy affected the majority of the data in the figure.

Flame Color in Zero Gravity

Figure 17 presents flame color observations made during the zero-gravity tests. Air-flow Reynolds number is plotted versus fuel Reynolds number for each of the three nozzles. As a general rule, flame color varied from the extinguished cases to the lift limit in the following order: (1) orange, (2) yellow, (3) blue. Yellow and blue colors were typically seen for all the normal-gravity flames. In the fuel Reynolds number range of 60 to 85, the zero-gravity flame color changed from orange to yellow at an Re_a of about 70 to 90 for the 0.305-cm nozzle, an Re_a of about 35 to 40 for the 0.186-cm nozzle, and an Re_a of about 0 to 3 for the 0.015-cm nozzle.

An air-flow Reynolds number range wherein a steady zero-gravity flame was not sustained, labeled "extinguished" on the figure, occurred only with the two largest nozzles studied. On the 0.186-cm nozzle, the demarcation between extinguished and steady zero-gravity flames occurred at an Re_a of about 11 or an air-flow velocity of about 7 cm/sec. On the 0.305-cm nozzle, the demarcation occurred at an Re_a of about 28 or an air flow velocity of about 9 cm/sec. It is therefore concluded from these data that methane flame extinguishment can be prevented for the test conditions run with a rather small minimum air flow velocity of about 10 cm/sec.

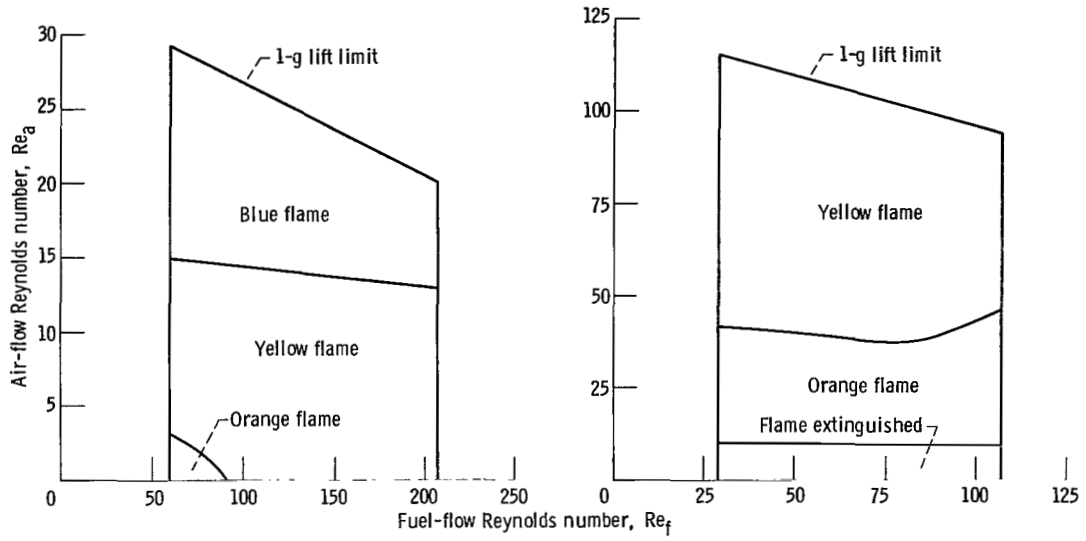

(a) Fuel-nozzle inside radius, R_o, 0.051 cm. (b) Fuel-nozzle inside radius, R_o, 0.186 cm.

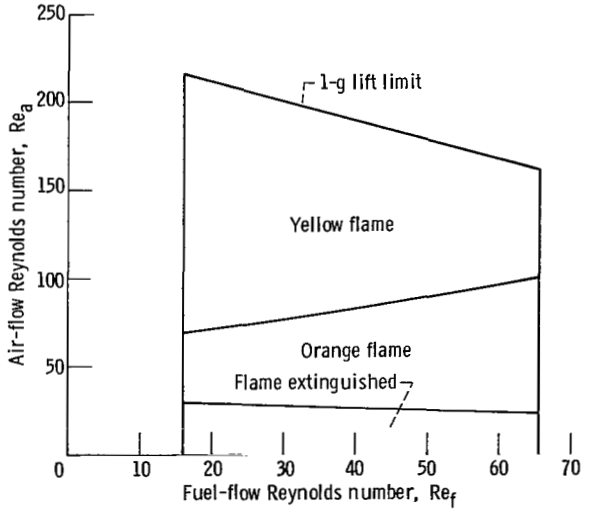

(c) Fuel-nozzle inside radius, R_o, 0.305 cm.

Figure 17. - Flame colors in zero-gravity.

Summary of Results

An experimental investigation was performed on methane laminar-jet diffusion flames with coaxial forced air flow to examine the geometry and appearance of normal-gravity, zero-gravity, and inverted-gravity flames. Fuel nozzles ranged in size from 0.051- to 0.305-cm inside radius, while the convergent air nozzle had a 1.4-cm inside radius at the fuel exit plane. Fuel flows ranged from 1.55 to 10.3 cm^3/sec, and air flows from 0 to 597 cm^3/sec.

The following are the principal results of this investigation:

1. In a test configuration without forced air flow, comparisons of normal-gravity, zero-gravity, and inverted-gravity flames with given fuel flow rates and fuel nozzles showed that zero-gravity flames possessed the longest axial lengths and widest flame radii. Normal-gravity flames were longer than inverted-gravity flames, and inverted-gravity flames were wider than normal-gravity flames.

2. The maximum flame radius for inverted-gravity flames without forced air flow was found to be

$$R_M/R_o = 8.55 - 3.7 \log(\tau_f)$$

where

R_M maximum flame radius, cm
R_o fuel-nozzle inside radius, cm
τ_f R_o times 1000 divided by the average fuel velocity, V_f, msec

3. In the range of fuel velocities tested (5 to 2000 cm/sec), the flame began to lift off the nozzle and was blown out at higher coaxial air flow rates for inverted-gravity flames than for normal-gravity flames.

4. The zero-gravity, axial-flame-length data were correlated by the following equation:

$$L/(R_o Re_f) = 0.48 + 3.92/(Re_a + 8)$$

where

R_o fuel-nozzle inside radius, cm
Re_f fuel-flow Reynolds number
Re_a air-flow Reynolds number

Using a computer program developed under NASA contract NAS3-14378, the zero-gravity axial length was predicted to within 1.3 percent of the actual data.

5. The normal-gravity, axial-flame-length data were correlated by the following equation:

$$L/(R_o Re_f) = 0.56 - .0005\, Re_a$$

The aforementioned computer program consistently predicted larger normal-gravity and axial flame lengths than were observed.

6. The zero-gravity, maximum flame radii were correlated by the following equation:

$$R_M/R_o = 2.4 + 4.75 \log(\tau_a/\tau_f)$$

where

$\tau_a = R_W/V_a$
$\tau_f = R_o/V_f$

The computer model consistently predicted larger zero-gravity, maximum flame radii than were observed, with an average error of 55 percent.

7. The normal-gravity, maximum flame radii were correlated by the following equation:

$$R_M/R_o = 1.5 + 3.0 \log(\tau_a/\tau_f)$$

8. It was shown that methane flame extinguishment upon entering zero gravity can be prevented with rather small minimum air flow velocities of 10 cm/sec.

Lewis Research Center
National Aeronautics and Space Administration
Cleveland, Ohio, October 3, 1980

References

1. Andracchio, Charles R.; and Aydelott, John C.: Comparison of Flame Spreading over Thin Flat Surfaces in Normal Gravity and Weightlessness in an Oxygen Environment. NASA TM X-1922, 1970.
2. Andracchio, Charles R.; and Cochran, Thomas H.: Gravity Effects on Flame Spreading over Solid Surfaces. NASA TN D-8228, 1976.
3. Cochran, Thomas H.; et al.: Burning of Teflon-Insulated Wires in Supercritical Oxygen at Normal and Zero Gravities. NASA TM X-2174, 1971.
4. Cochran, Thomas H.; and Masica, William J.: Effects of Gravity on Laminar Gas Jet Diffusion Flames. NASA TN D-5872, 1970.
5. Cochran, Thomas H.; and Masica, William J.: An Investigation of Gravity Effects on Laminar Gas-Jet Diffusion Flames. Thirteenth Symposium (International) on Combustion. Combustion Institute, 1971, pp. 821-829.
6. Cochran, Thomas H.: Experimental Investigation of Laminar Gas Jet Diffusion Flames in Zero Gravity. NASA TN D-6523, 1972.
7. Edelman, Raymond B.; Fortune, Owen F.; and Weilerstein, Gertrude: An Analytical Study of Gravity Effects on Laminar Diffusion Flames. (GASL-TR-771, General Applied Science Labs; NASA Contract NAS3-14378.) NASA CR-120921.
8. Edelman, Raymond B.; et al.: An Analytical and Experimental Investigation of Gravity Effects upon Laminar Gas Jet Diffusion Flames. Fourteenth Symposium (International) on Combustion. Combustion Institute, 1973, pp. 399-412.
9. Haggard, John B., Jr.; and Cochran, Thomas H.: Stable Hydrocarbon Diffusion Flames in a Weightless Environment. Combus. Sci. Technol., vol. 5, no. 6, Aug. 1972, pp. 291-298.
10. Haggard, John B., Jr.; and Cochran, Thomas H.: Hydrogen and Hydrocarbon Diffusion Flames in a Weightless Environment. NASA TN D-7165, 1973.
11. Kimura, Itsuro; and Ukawa, Haruo: A Study of the Combustion of Laminar Fuel Jets. Translated from Trans. of Jap. Soc. of Mech. Engrs., vol. 27, 1961, pp. 736-746. NASA TT F-13459, 1971.
12. Fluid Flow Instrumentation, Heat Flux System, Model 1010A Instruction Manual, Thermo-Systems, Inc., Minneapolis, Minnesota.
13. Patankar, S. V.; and Spalding, D. B.: Heat and Mass Transfer in Boundary Layers. Second ed., Intertex Books (London), 1970, Appendix B.

TABLE I. - ZERO-GRAVITY TEST DATA

Inside radius of fuel nozzle, R_o, cm	Fuel flow rate, Q_f, cm^3/sec	Air flow rate, Q_a, cm^3/sec	Steady-state, axial length of flame, L, cm	Steady-state, maximum radius of flame, R_M, cm	Run
0.051	1.55	0	2.91	0.62	1
		40.9	2.11	.42	2
		104.3	1.83	.34	3
		209.7	1.84	.28	4
	2.68	0	4.80	0.67	5
		17.3	4.95	.67	6
		58.6	3.68	.55	7
		226.8	2.93	.40	8
	5.35	0	9.91	0.68	9
		23.6	9.84	.64	10
		68.8	8.54	.59	11
		115.2	8.21	.55	12
		169.1	[a]7.50	.88	13
0.186	2.71	0	-----	----	14
		7.9	-----	----	15
		23.6	-----	----	16
		58.6	3.01	0.70	17
		130.2	2.78	.50	18
		157.3	2.54	.52	19
		296.2	2.65	.32	20
		387.0	2.42	.40	21
	5.39	0	-----	----	22
		23.6	-----	----	23
		40.9	7.61	1.39	24
		58.7	8.10	1.14	25
		130.2	6.62	.79	26
		300.1	5.30	.54	27
	10.30	0	-----	----	28
		7.9	-----	----	29
		23.6	-----	----	30
		40.9	8.63	1.40	31
		58.6	13.91	1.33	32
		93.6	13.18	1.19	33
		130.2	(b)	1.21	34
		209.7	(b)	.76	35
0.305	2.68	23.6	-----	----	36
		58.6	2.82	0.82	37
		130.2	2.77	.58	38
		296.2	2.64	.45	39
	5.24	0	-----	----	40
		23.6	-----	----	41
		40.9	-----	----	42
		58.6	7.79	1.41	43
		209.7	5.44	.67	44
	10.30	0	-----	----	45
		23.6	-----	----	46
		40.9	2.71	1.57	47
		58.6	6.78	1.61	48
		130.2	9.45	1.03	49
		209.7	8.47	.87	50

[a]Flame lifted off the nozzle.

[b]Flame out of field of view of the camera.

TABLE II. - NORMAL-GRAVITY TEST DATA

Inside radius of fuel nozzle, R_o, cm	Fuel flow rate, Q_f, cm^3/sec	Air flow rate, Q_a, cm^3/sec	Average axial length of flame, L, cm	Maximum radius of flame, R_M, cm	Run
0.051	1.55	0	1.83	0.32	1
		40.9	1.60	.28	2
		104.3	1.63	.30	3
		209.7	1.67	.28	4
	2.68	0	3.21	0.38	5
		17.3	3.27	.33	6
		58.6	2.88	.31	7
		226.8	2.78	.29	8
	5.35	0	7.13	0.39	9
		23.6	7.09	.38	10
		68.8	6.62	.37	11
		115.2	6.82	.36	12
		169.1	[a]6.44	.47	13
0.186	2.71	0	2.68	0.38	14
		7.9	2.67	.34	15
		23.6	2.56	.30	16
		58.6	2.52	.29	17
		130.2	2.55	.25	18
		157.3	2.47	.33	19
		296.2	2.49	.40	20
		387.0	2.38	.43	21
	5.39	0	5.67	0.68	22
		23.6	4.94	.65	23
		40.9	5.18	.55	24
		58.7	5.21	.55	25
		130.2	5.30	.44	26
		300.1	4.87	.44	27
	10.30	0	10.28	0.90	28
		7.9	9.93	.91	29
		23.6	9.98	1.04	30
		40.9	10.38	.94	31
		58.6	10.98	.85	32
		93.6	10.32	.87	33
		130.2	11.93	.80	34
		209.7	12.25	.60	35
0.305	2.68	23.6	2.54	0.44	36
		58.6	2.38	.42	37
		130.2	2.64	.37	38
		296.2	2.35	.41	39
	5.24	0	5.11	0.74	40
		23.6	5.44	.76	41
		40.9	5.26	.64	42
		58.6	5.83	.65	43
		209.7	5.43	.48	44
	10.30	0	7.83	1.13	45
		23.6	8.81	1.07	46
		40.9	7.06	1.10	47
		58.6	9.17	.99	48
		130.2	8.22	.66	49
		209.7	7.74	.51	50

[a]Flame lifted off the nozzle.

TABLE III. - INVERTED-GRAVITY TEST DATA

Inside radius of fuel nozzle, R_o, cm	Fuel flow rate, Q_f, cm^3/sec	Air flow rate, Q_a, cm^3/sec	Average axial length of flame, L, cm	Maximum radius of flame, R_M, cm	Run
0.051	1.55	0	1.24	0.49	1
		40.9	1.31	.52	2
		93.6	1.42	.56	3
		149.5	1.47	.65	4
		209.7	1.53	.66	5
		274.1	1.59	.66	6
		387.0	1.98	.45	7
	2.68	0	2.79	0.59	8
		40.9	2.79	.59	9
		93.6	2.82	.61	10
		149.5	2.65	.71	11
		209.7	2.79	.71	12
		274.1	2.78	.86	13
		387.0	3.05	.84	14
	5.35	0	6.65	0.70	15
		40.9	6.33	.65	16
		93.6	6.06	.65	17
		149.5	5.55	.69	18
		209.7	5.00	.68	19
		274.11	5.23	.80	20
		387.0	5.16	1.11	21
0.186	2.58	0	0.77	0.87	22
		23.6	1.29	1.06	23
		58.6	1.21	1.76	24
		93.6	1.27	1.70	25
		130.2	1.24	1.14	26
		157.3	1.35	1.21	27
		209.7	1.45	1.68	28
		296.2	1.75	1.57	29
		387.0	2.11	.80	30
		527.0	2.45	.49	31
	5.39	0	1.31	0.98	32
		40.9	2.00	1.33	33
		93.6	2.06	1.51	34
		149.5	2.30	1.97	35
		209.7	2.35	1.56	36
		274.1	2.51	1.69	37
		341.0	2.50	1.76	38
		387.0	2.70	1.57	39
	10.30	0	3.32	1.25	40
		40.9	3.11	1.14	41
		93.6	3.85	1.33	42
		149.5	3.79	1.65	43
		209.7	4.28	1.82	44
		274.1	4.11	1.92	45
		341.0	4.71	2.26	46
		387.0	4.48	2.18	47
0.305	2.68	0	0.57	1.00	48
		40.9	.75	1.15	49
		93.6	.75	1.15	50
		149.5	.91	1.05	51
		209.7	1.05	1.05	52
		274.1	1.20	.97	53
		387.0	1.56	.83	54
		597.8	2.19	.46	55
	5.24	0	0.82	1.23	56
		40.9	1.21	2.13	57
		93.6	1.41	1.64	58
		149.5	1.51	1.55	59
		209.7	1.63	1.50	60
		274.1	1.75	1.57	61
		387.0	2.29	1.46	62
		597.8	3.06	1.07	63
	10.30	0	1.63	1.61	64
		40.9	2.22	2.64	65
		93.6	2.38	2.38	66
		149.5	2.44	2.24	67
		209.7	2.47	2.11	68
		274.1	2.55	2.05	69
		387.0	2.40	2.09	70
		597.8	3.74	1.96	71

1. Report No. NASA TP-1841	2. Government Accession No.	3. Recipient's Catalog No.
4. Title and Subtitle FORCED AND NATURAL CONVECTION IN LAMINAR-JET DIFFUSION FLAMES		5. Report Date June 1981 6. Performing Organization Code 506-55-22
7. Author(s) John B. Haggard, Jr.		8. Performing Organization Report No. E-487 10. Work Unit No.
9. Performing Organization Name and Address National Aeronautics and Space Administration Lewis Research Center Cleveland, Ohio 44135		11. Contract or Grant No. 13. Type of Report and Period Covered Technical Paper
12. Sponsoring Agency Name and Address National Aeronautics and Space Administration Washington, D.C. 20546		14. Sponsoring Agency Code
15. Supplementary Notes		

16. Abstract

An experimental investigation was conducted on methane, laminar-jet, diffusion flames with coaxial, forced air flow to examine flame shapes in zero-gravity and in situations where buoyancy aids (normal-gravity flames) or hinders (inverted-gravity flames) the flow velocities. Fuel nozzles ranged in size from 0.051- to 0.305-cm inside radius, while the coaxial, convergent, air nozzle had a 1.4-cm inside radius at the fuel exit plane. Fuel flows ranged from 1.55 to 10.3 cm^3/sec and air flows from 0 to 597 cm^3/sec. A computer program developed under a previous government contract was used to calculate the characteristic dimensions of normal- and zero-gravity flames only. The results include a comparison between the experimental data and the computed axial flame lengths for normal gravity and zero gravity which showed good agreement. Inverted-gravity flame width was correlated with the ratio of fuel nozzle radius to average fuel velocity. Flame extinguishment upon entry into weightlessness was studied, and it was found that relatively low forced-air velocities ($\approx$10 cm/sec) are sufficient to sustain methane flame combustion in zero gravity. Flame color is also discussed.

17. Key Words (Suggested by Author(s))	18. Distribution Statement
Convection Diffusion flames Zero gravity Spacecraft safety	Unclassified - unlimited STAR Category 34

19. Security Classif. (of this report)	20. Security Classif. (of this page)	21. No. of Pages	22. Price*
Unclassified	Unclassified	23	A02

* For sale by the National Technical Information Service, Springfield, Virginia 22161

NASA-Langley, 1981

10 1 1U,D, 052081 S00903DS
DEPT OF THE AIR FORCE
AF WEAPONS LABORATORY
ATTN: TECHNICAL LIBRARY (SUL)
KIRTLAND AFB NM 87117